Accepted Manuscript

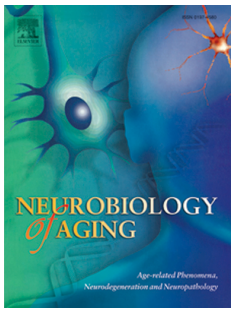

Laser-captured microglia in the Alzheimer's and Parkinson's brain reveal unique regional expression profiles and suggest a potential role for hepatitis B in Alzheimer's brain.

Diego Mastroeni, Jennifer Nolz, Shobana Sekar, Elaine Delvaux, Geidy Serrano, Lori Cuyugan, Winnie S. Liang, Thomas G. Beach, Joseph Rogers, Paul D. Coleman

PII: S0197-4580(17)30358-5

DOI: 10.1016/j.neurobiolaging.2017.10.019

Reference: NBA 10075

To appear in: *Neurobiology of Aging*

Received Date: 7 July 2017

Revised Date: 2 October 2017

Accepted Date: 22 October 2017

Please cite this article as: Mastroeni, D., Nolz, J., Sekar, S., Delvaux, E., Serrano, G., Cuyugan, L., Liang, W.S., Beach, T.G., Rogers, J., Coleman, P.D., Laser-captured microglia in the Alzheimer's and Parkinson's brain reveal unique regional expression profiles and suggest a potential role for hepatitis B in Alzheimer's brain., *Neurobiology of Aging* (2017), doi: 10.1016/j.neurobiolaging.2017.10.019.

Laser-captured microglia in the Alzheimer's and Parkinson's brain reveal unique regional expression profiles and suggest a potential role for hepatitis B in Alzheimer's brain.

Diego Mastroeni[a,b*], Jennifer Nolz[a], Shobana Sekar[c], Elaine Delvaux[a], Geidy Serrano[b], Lori Cuyugan[c], Winnie S. Liang[c], Thomas G. Beach[b] Joseph Rogers[d], and Paul D. Coleman[a,b]

[a] Biodesign, ASU-Banner Biodesign Neurodegenerative Disease Research Center, and School of Life Sciences, Arizona State University, Tempe, AZ 85287

[b] Banner Sun Health Research Institute, 10515 West Santa Fe Drive, Sun City, AZ 85351.

[c] Translational Genomics Institute, 445 N. Fifth Street Phoenix, Arizona 85004

[d]SRI International, 333 Ravenswood Avenue, Menlo Park, CA 94025

*Corresponding Author: Diego.Mastroeni@asu.edu

Abstract

Expression array data from dozens of laboratories, including our own, show significant changes in expression of many genes in Alzheimer's (AD) patients compared to normal controls (NC). These data typically rely on brain homogenates, and information about transcripts specific to microglia and other CNS cell types, which far outnumber microglia-specific transcripts, is lost. We therefore employed single cell laser capture methods to assess the full range of microglia-specific expression changes that occur in different brain regions (substantia nigra and hippocampus CA1), and disease states (AD, Parkinson's disease (PD), and NC). Two novel pathways, neuronal repair and viral processing were identified. Based on KEGG analysis, one of the most significant viruses was hepatitis B virus (HBV) (FDR<.00000001). Immunohistochemistry with HBV core antibody in HBV-positive control, amnestic mild

cognitive impairment, and AD cases, showed increased HBV immunoreactivity as disease pathology increases. These results are the first, to our knowledge, to show regional differences in human microglia. In addition, these data reveal new functions for microglia, and suggest a novel risk factor for AD.

Key Words: Microglia; Alzheimer's disease; Parkinson's disease, Laser Capture; RNA sequencing; Virus; Synapse

1. INTRODUCTION

Microglial cells are well accepted to be resident innate immune cells within the CNS and key regulators of the inflammatory cascade (Farina et al., 2007; Rivest, 2009; Solito and Sastre, 2012). They have been shown to release neurotoxic inflammatory factors, as well as factors that regulate the extent and duration of the inflammatory response (reviewed in (Rogers et al., 1996; Wyss-Coray and Rogers, 2012). These data have prompted several clinical studies to alter microglial actions such as pro-inflammatory cytokine secretion in Alzheimer's disease (AD), but none of these efforts has been successful to date (reviewed in (Wyss-Coray and Rogers, 2012). One reason may be the choice of a single inflammatory mediator (e.g., TNF-α (Tobinick, 2009)) as a drug target, whereas microglia are known to express a virtual textbook of destructive molecules when activated (Alam et al., 2016; Wyss-Coray and Rogers, 2012). A complete, microglia-specific expression profile might therefore indicate upstream, more global pathways as drug targets. Likewise, microglia clearly undergo distinct immunohistochemical changes indicative of different activation states in response to various environmental stressors (Kettenmann et al., 2011), but a consensus view of the underlying mechanisms, particularly with

respect to differences that occur in different brain regions, has not been achieved. Here, again, a more complete portrait of microglia-specific gene expression would obviously be helpful.

Unfortunately, a full description of changes in microglial gene expression cannot be elucidated in large-scale expression arrays that rely on brain homogenates, since cell specificity information is lost with such preparations. Although some specificity is afforded by genes whose expression is relatively unique to microglia, the number of such cell-specific genes is actually quite small compared to the thousands of genes that microglia share in common with other CNS cell classes. Doorn et al. (2015) combined density gradient centrifugation with fluorescence-activated cell sorting (FACS) to purify microglia from brain homogenates prior to array expression analyses. Although this well-conceived approach proved useful in demonstrating novel brain regional differences in microglia expression profiles, the extent to which such profiles might be distorted by the processes of dissociation, centrifugation, and cell sorting remains unclear.

To overcome these challenges, we have used single-cell laser capture methods to compare isolated microglia from normal elderly control (NC) patients with isolated microglia from two different disease states, AD and Parkinson's disease (PD), in two different pathologically-impacted brain regions in each disease: hippocampus CA1 and substantia nigra (SN). By including only microglia, the full panoply of gene expression changes in this cell type and their potential pathologic relevance may be recognized. Our results demonstrate significantly enhanced pathways in microglia that might otherwise have been obscured in homogenate studies by lack of change in other cell types. This was particularly true with respect to changes in neuronal repair genes, as well as an unexpected pathway, viral processing, that was

detected in CA1 AD microglia. An overview of our unbiased approach and work flow can be found in Supplementary Figure 1.

2. METHODS:

2.1. Tissue collection

10μm frozen, unfixed and 40μm 4% buffered paraformaldehyde-fixed midbrain and limbic regions containing SN and CA1 of hippocampus, respectively, were obtained from the tissue bank at Banner Sun Health Research Institute, a National Institute on Aging AD Center. For laser capture microdissection (LCM) studies, the samples were from clinically-diagnosed and neuropathologically-confirmed late-onset AD cases (n=6) with a mean age of 74.6 ± 6.8 years, healthy elderly control (NC) cases (n=6) with a mean age of 73.6 ± 6 years, and PD cases (n=6) with a mean age of 74.6 ± 15.6 years (Supplementary Table 1). AD and PD cases were devoid of pathology other than that of their respective diseases (i.e., no material overlapping pathology), and NC cases showed no material AD or PD pathology beyond that normally associated with age. All cases in the LCM study were male in order to avoid gender-related variability. For immunohistochemical studies, we selected 4 male, HBV-positive, Braak Stage V AD cases with a mean age of 78.75± 4.5 years, and a mean postmortem interval (PMI) of 1.94 hours ± 12 min; 3 male, HBV-positive, Braak I NC cases with a mean age of 80.5 ± 7.7 years and a mean PMI of 1.9 hours ± 12 min; and 2 male, HBV-positive, Braak IV MCI cases , with a mean age of 79 ± 2.8 years and a mean PMI of 2.9 hours ± 1 hours (Supplementary Table 1).

2.2. Laser capture of microglia

As previously published (Mastroeni et al., 2017), frozen midbrain and limbic regions containing the SN and hippocampus CA1, respectively, were sectioned at 8-10µm. The sections were then mounted onto polyethylene naphthalate membrane (PEN) slides, fixed in ice-cold acetone/ethanol for 10 min on ice, and washed in ice-cold 1X PBS (Phosphate buffered saline). After blocking in 1% hydrogen peroxide for 2 min, followed by 3 quick dips in ice cold 1X PBS, the sections were placed in a 1:500 dilution of primary antibody LN3 (Sigma) in 1X PBS supplemented with 50U RNAseOUT (Invitrogen) for 10 min at room temperature. In brain, LN3 is a specific marker for activated microglia (Carpenter et al., 1993; Parachikova et al., 2007) that does not stain neurons or other glial types (Walker and Lue, 2015). After incubation, sections were washed 3X in 1X PBS, followed by incubation with avidin (1:300)-biotin (1:300) complex (Vector) in 1X PBS for 10 min at room temperature (RT). Sections were washed 3X in 50mM Tris buffer and immersed in DAB solution (9.3 ml 50mM Tris, 200µl of 5mg/ml DAB, 500 µl saturated nickel, and 4 µl of 1% hydrogen peroxide) for 5 min, followed by two quick rinses in 50mM Tris to stop the reaction. Immediately after staining, sections were dipped in 100% ethanol, allowed to dry, and loaded onto a Leica AS-LMD laser capture microscope. After stage and objective calibration, 600 LN3 positive cells were captured from each section using 20X magnification (Supplementary Fig. 2). Individual microglial cells were cut and dropped into an inverted microcentrifuge cap containing 50µl buffer RLT (RNeasy Micro Kit (Qiagen) and 1% β-Mercaptoethanol. For each subject, 600 microglia were captured in each of two serial sections of CA1 and an additional 600 microglia were captured in each of two serial sections of the SN, providing a total sample of 21,600 microglia over the 6 AD, 6 PD, and 6 NC cases. In order to determine if immunohistochemical experiments had an effect on RNA quality, all samples were scraped after microdissection and tested on a Bioanalyzer. All brain samples had RIN values

greater than 6.5 (supplementary Table 1), the point at which RNA is generally considered to be of acceptable quality for molecular research studies (Durrenberger et al., 2010).

2.3. Quantitative RT-PCR of immunolabeled, laser-captured microglia

Total RNA was extracted using RNeasy Micro Kit (Qiagen) and completed following the manufacturer's protocol, including DNase treatment. RNA was reverse transcribed using High Capacity cDNA Reverse Geneion Kits (Life Technologies/Applied Biosystems). The resulting cDNA was pre-amplified using TaqMan PreAmp Master Mix (Life Technologies/Applied Biosystems), after which quantitative real time PCR was performed in triplicate on the iCycler iQ (Bio-Rad) with TaqMan Gene Expression Assays (Life Technologies/Applied Biosystems). To assess microglial purity of the samples, the triplicate QPCR expression data were evaluated for relative expression levels of the microglia-specific transcripts CD14, CD68, and CD11b (Liu et al., 2005; Walker and Lue, 2015); the astrocyte-specific transcript GFAP (Mandybur and Chuirazzi, 1990); and the neuron-specific transcripts CHRM1, SYP, and MAP2 (Cahoy et al., 2008; Liang et al., 2008). The results clearly demonstrated high specificity for microglia, with minimal GFAP or neuronal contamination (Supplementary Fig. 3).

2.4. RNA sequencing: *RNAseq Library Preparation:* Total RNA was employed to generate whole transcriptome libraries for RNA sequencing. Using the Nugen Ovation RNA-Seq System v2, total RNA was used to generate double stranded cDNA, which was subsequently amplified using Nugen's SPIA linear amplification process. Amplified products were cleaned using Qiagen's QIAquick PCR Purification Kit and quantitated using Invitrogen's Quant-iT Picogreen. 1 ng of amplified cDNA was fragmented on the Covaris E210 to a target size of 300bp. Kapa Biosystems' Library Preparation Kit and Illumina adapters and sequencing primers were used for

preparing libraries from amplified cDNA. Final libraries were quantified using the Agilent Bioanalyzer and Life Technologies/Invitrogen Qubit. *Paired End Sequencing:* Libraries with a 1% phiX spike-in were used to generate clusters on HiSeq Paired End v3 flowcells on the Illumina cBot using Illumina's TruSeq PE Cluster Kit v3. Clustered flowcells were sequenced by synthesis on the Illumina HiSeq 2000 using paired-end technology and Illumina's 200 cycle TruSeq SBS Kit, extending to 83 bp for each of two reads and a 7bp index read. Approximately 250-300 Gigabases (Gb) of reads were generated per flowcell based on Illumina's published throughput. *Quality Control Steps:* During library preparation, electrophoretically separated DNA fragments were analyzed on a TAE gel to verify fragmentation. Final libraries were run on a Bioanalyzer to verify sizes and quantitate libraries prior to sequencing. During and following sequencing, we evaluated the total amount of Q30 data generated per library, total number of reads generated, and the total number of mappable reads. *Data analysis:* Following completion of sequencing, we initiated an automated pipeline for NGS analysis. At each step within the pipeline, statistics files were created to ensure that all processes had been completed and files were uncorrupted. Early within the pipeline, several additional checks were invoked including estimates of overall coverage on a library, evenness of a library, quality of bases, and contamination checks. Standardized file formats, multiple quality control checks, automated processing, scheduled releases of sequence data, sequencing alignments, variant calls, and centralized primary data processing are built into the pipeline. Reads first went through a series of quality control steps quantifying for biases at any given base, and were then parsed by barcode into independent FASTQ files. FASTQ alignments were aligned with TopHat (Trapnell et al., 2009; Trapnell et al., 2012). Alignment produced single BAM files containing both aligned and unaligned data. For analysis, TopHat and Cufflinks were used to assemble reads into genes, and

HTSeq was used to generate counts data from Cufflinks' output. DESeq2 calculated normalized read counts for each gene/gene and used a generalized linear model to evaluate differential expression between sample groups while accounting for biological variance. DESeq2 uses a Wald statistic as a measure of significance. The Benjamin and Hochberg False Discovery Rate (FDR) was used for multiple testing corrections. Genes with an adjusted or corrected significance criterion of $P < 0.05$ were evaluated. Variability in the number of reads was accounted for during normalization of read counts. In total, we collected data from samples that gave at least 50 million reads; samples with lower than 50 million reads were omitted (Supplementary Fig. 4). Intronic sequences were analyzed using an unbiased approach to evaluate changes in expression of all RNAs. Final libraries were run through the Bioanalyzer to verify sizes and to quantitate libraries prior to sequencing. During and following sequencing, we evaluated the total amount of Q30 data generated per library, total number of reads generated, and the total number of mappable reads. Additional quality control and picard tool metrics can be found in Supplementary Figs. 5 and 6. For pathway analysis (2D-single cluster analysis) we employed Cytoscape network visualizer and string software (Lopes et al., 2010; Szklarczyk et al., 2017).

2.5. Immunohistochemistry for viral antigens

Midbrain and limbic regions containing SN and hippocampus CA1, respectively, were fixed with 4% buffered paraformaldehyde and sectioned at 40µm. Free-floating sections were washed in PBS/Triton X-100 (PBST), blocked in 1% hydrogen peroxide followed by 1h incubation in 3% bovine serum albumin (BSA), then incubated in anti-hepatitis B virus (HBV) primary antibody (Anti-HBV, ThermoFisher Scientific, cat# RB1413A, and DAKO Cat# BO586) (Alarcon et al., 2016; Di Scala et al., 2016; Murray et al., 1984; Stahl et al., 1982) at a concentration of 1:1000,

4ºC, overnight. Primary antibody solutions contained 0.25% BSA to inhibit non-specific binding. After incubation, sections were washed, incubated in biotinylated, species-specific secondary antibodies (Vector) for two hours at RT, washed 3X in PBST and incubated in avidin-biotin complex (ABC, Pierce) for 30 min. Following incubation with ABC, sections were washed 2X in 50 mM Tris buffer, immersed in DAB solution (500µl 5mg/ml DAB, 2 ml saturated nickel, 10µl 1% hydrogen peroxide), and brought to a final volume of 50 ml with 50 mM Tris buffer), followed by two quick rinses in 50 mM Tris to stop the reaction. AD, MCI, and NC sections were immunoreacted simultaneously using netwells in well-less plates. Sections were mounted with Permount (Pierce). Immunostained tissue sections were examined on an Olympus IX70 microscope. The findings were documented photographically with an Olympus DP-71 color digital camera. To provide estimates of viral immunoreactivity, bright field intensity analysis was performed using Image J software (Image J, U.S. National Institutes of Health, Bethesda, MD; imagej.nih.gov/ij/). Significance was determined using a 2-tailed Student t-test and declared significant at a p-value < 0.05. Intensity measurements were corrected for background differences by dividing the measured intensities with the average intensity of a background region (e.g., a cell-free region such as the hippocampal white matter) in each section. Correlation analyses were carried out by calculating the Pearson's correlation coefficient (rp). All statistical calculations were performed using STATA 11 (StataCorp, College Station, TX) or the Statistical Package for the Social Sciences (SPSS 17; SPSS Inc, Chicago, IL).

3. RESULTS

3.1. Brain regional differences in microglia expression profiles

NC cases provided the clearest opportunity to discern brain regional differences in microglia

expression profiles since they were relatively unconfounded by regional differences in pathology associated with disease (e.g., CA1 in AD, SN in PD). We began by selecting microglial transcripts that exhibited significant ($p<.05$) log2 fold changes in NC CA1 versus NC SN. Hierarchical clustering analysis of the log2 fold changes of the significantly altered transcripts is summarized in the heat map of Fig. 1, and shows a striking dissimilarity between brain regions. Categorical data (Fig. 1., cluster 1 versus cluster 2) suggested unexpected biological processes that were upregulated in CA1 microglia relative to SN microglia, with the top three being nervous system development, regulation of neuronal synaptic plasticity, and neurogenesis. Although these are functions that one might superficially associate with neurons, control assays (Supplementary Fig. 3) showed virtually no material neuronal contamination of the laser-captured microglia samples. Additionally, cluster 3 versus cluster 4 analyses showed downregulation of mitochondria-associated transcripts in CA1 relative to SN (GO:0007399, GO:004533, GO:0046034). Many of the effected pathways, especially mitochondrial, had overlapping genes within the same pathways. Collectively, the data indicate that even in the normal elderly brain, where differential pathology in limbic versus midbrain structures should not play a role, microglia expression patterns differ regionally and include unexpected neuronal and neuronal repair functions that may have been obscured by analyses of brain homogenates. In fact, some 48% of the significantly altered CA1 microglia transcripts in the present experiments were either not significant or not detectable in our previous studies of hippocampal homogenates (Berchtold et al., 2013; Berchtold et al., 2008; Berchtold et al., 2014; Mastroeni et al., 2016) and comparisons to GEO database www.ncbi.nlm.nih.gov/geo (accession no. GSE11882). These results highlight the value of LCM methods, since most of the undetected microglia transcript changes were in functions common to multiple CNS cell classes that could not be specifically

ascribed to microglia without LCM. Moreover, in a homogenate sample, such changes could also be swamped by lack of change or opposite changes in the other cell types. The complete dataset for the present study can be found at the National Institute on Aging Genetics of Alzheimer's disease (NIAGADS) data storage site under accession number NG00057.

3.2. Disease-state differences in microglia expression profiles

In AD CA1 there were 366 significantly altered transcripts compared to NC CA1 (Fig. 2A), whereas in PD CA1 there were 409 significantly altered transcripts compared to NC CA1 (Fig. 2B). Perhaps consistent with the fact that hippocampus CA1 is one of the most pathologically vulnerable brain structures in AD (Padurariu et al., 2012), whereas it is relatively spared of pathology in PD, only 7% of the significantly altered transcripts were the same for AD and PD. Hierarchical cluster analysis of the significantly altered AD transcripts in CA1 revealed four expression clusters in which ~60% of the transcripts were up-regulated and ~40% were down-regulated relative to NC microglia (Fig. 2A). Three clusters were observed for PD microglia, with ~55% up-regulated and ~45% down-regulated transcripts compared to NC microglia (Fig. 2B). Pathway analysis of AD versus NC CA1 identified twenty-five pathways (Fig 2C). The top five pathways were thyroid hormone synthesis, icosanoid metabolic process, regulation of viral processes, negative regulation of homotypic cell-cell adhesion, and negative regulation of protein phosphorylation. In contrast, PD CA1 microglia exhibited nineteen unique pathways compared to NC cases (Fig 2D). The top five affected pathways in PD were aldosterone synthesis and secretion, positive regulation of protein complex assembly, focal adhesion assembly, tonic smooth muscle contraction, and positive regulation of reactive oxygen species biosynthetic processes. Further analysis of the top 100 significantly ($p<.01$) altered transcripts in AD CA1 compared to control and the top 100 transcripts in PD CA1 compared to control showed only 6

overlapping transcripts (*GLB1L2, INTS9, LRRC46, MOCS1, OAS3, and SRGAP3-AS2*) for the two disorders, all of which have regulatory roles in RNA processing. A complete list of all significant transcripts represented in the pathway analysis can be found in Supplementary Table 2.

To further assess disease-state differences, we also compared expression profiles of AD CA1 versus AD SN microglia and PD CA1 versus PD SN microglia. AD cases had 104 significantly altered transcripts in the pathologically-vulnerable CA1 compared to the AD SN, a brain region that is typically spared in AD (Fig. 3A). PD cases had 313 significantly altered transcripts in the pathologically vulnerable SN compared to PD CA1, a brain region that is typically spared from PD pathology (Fig. 3B). Of the 417 total significantly altered transcripts in AD and PD, only 7 overlapped: *ACKR2, ANK1, CCDC64, CHPT1, CMTM5, GPR17* and *NHLRC3,* all of which are largely associated with axon guidance and chemotaxis mechanisms. Despite the lack of commonality in AD and PD microglial responses to regional pathology, pathway analysis of the significantly altered transcripts nonetheless identified up-regulation of the GO term synaptic transmission as the most highly upregulated pathway in both AD (FDR 9.4 E-05) and PD (FDR 1.22 E-07) CA1 relative to the SN. These findings again indicate that microglia may be involved in synaptic functions that go well beyond synaptic pruning (Paolicelli et al., 2011). Finally, a comparison of significantly altered transcripts in AD CA1 versus PD SN revealed only 2% overlap despite the fact that both AD CA1 and PD SN are high pathology areas for their respective diseases, including profuse microglial inflammatory activity (Alam et al., 2016).

Although it has become clear that microglial cells are capable of transforming from resting to activated and phagocytic states in multiple CNS disorders (Boche et al., 2013), the

present data also suggest that microglial alterations are more complex than simple alterations in their activation states. In fact, despite residing in known neurodegenerative, proinflammatory microenvironments, the AD CA1 and the PD SN (Alam et al., 2016), very few microglial transcripts in AD CA1 and PD SN were overlapping.

3.3. Expression of viral-associated transcripts in AD brain

Functional enrichment analysis of microglial transcripts that were differentially expressed in AD CA1 compared to NC CA1 (Table 1) predicted 224 GO terms with a false discovery rate of 0.05 or less (supplementary Table 3a). The most significant (FDR $=6.90^{-38}$) GO term was GO.0016032, viral processes. KEGG pathway analysis subsequently identified 16 relevant pathways (Supplementary Table 3B), the most significant of which were endocytosis (FDR=0.0007), hepatitis B virus (HBV) infection (FDR=0.0007), and Epstein-Barr virus infection (FDR=0.0002). By contrast, only 15 of the 65 differentially expressed AD CA1 microglia transcripts within GO.0016032 (viral processes) were significantly changed in PD CA1 microglia (Supplementary Fig. 8). Six percent of all differentially expressed transcripts in AD CA1 microglia were found to be associated with viral processes, whereas only 1% of PD CA1 microglial transcripts, and less than 1% of PD and AD SN microglial transcripts, were associated with viral processes (Fig. 4). Functional protein association analysis of viral-related transcripts in AD CA1 showed significant protein-protein enrichment ($p<1.11\ E\text{-}16$) among the 65 nodes (proteins) and 91 edges (which denote a known or predicted interaction) (Supplementary Fig. 9).

3.4. HBV-core brain immunoreactivity in HBV-positive subjects.

In order to confirm the ability of HBV to cross the blood brain barrier and be detected in the brains of HBV-positive individuals, we used immunohistochemical techniques. Representative

photomicrographs of HBV-core antibody immunoreactivity in CA1 of an HBV-positive, Braak I NC subject (Fig. 5A), HBV-positive, Braak IV MCI subject (Fig. 5B), and HBV-positive, Braak V AD case (Fig. 5C) illustrate the clear differences in disease states. Despite the fact that all the cases had been diagnosed with, and were serologically positive for HBV, NC cases showed only equivocal immunoreactivity for brain HBV, whereas AD cases exhibited robust, intracellular-punctate neuronal immunoreactivity and MCI cases had intermediate findings.

4. Discussion:

Previous studies of microglial gene expression have almost exclusively focused on the neuroinflammatory properties of these cells because, having employed brain homogenates, microglial specificity could only be definitively attributed to transcripts exclusively expressed by microglia—and almost all of these are inflammation related. As important as the role of microglia in AD and PD inflammation clearly is (Rogers et al., 2007), inflammation-related transcripts constitute only a small minority of the 20,000 or so protein-producing transcripts in a human microglial cell. Considering the potential importance of changes in these other, much more numerous microglial transcripts, we employed single-cell laser capture in order to assess the full panoply of microglial gene expression changes. Our results demonstrate that brain microglia exhibit substantially different gene expression patterns and profiles depending on the brain region assayed and the disease state of the cases. Importantly, however, the most significant changes were not, as expected, in inflammatory transcripts, but in transcripts related to neuronal repair (e.g., neuronal development, plasticity, and neurogenesis). Thus, by employing single cell laser capture methods that permit analysis of transcripts common to multiple brain cell types, our data suggest an important new class of functions for microglia, and

support and extend the growing recognition that microglia may play significant roles in nervous system development (Frost and Schafer, 2016; Schafer and Stevens, 2015), synaptic plasticity (Hong et al., 2016; Kettenmann et al., 2013; Paolicelli et al., 2011; Perry and O'Connor, 2010; Schafer and Stevens, 2015), and neurogenesis (De Lucia et al., 2016; Luo et al., 2016; Pikhovych et al., 2016; Shigemoto-Mogami et al., 2014; Sierra et al., 2010). In addition, we have, long emphasized that inflammation is a double-edged sword, with both destructive and restorative arms (Rogers et al., 2007). The present findings are consistent with this view and suggest that more attention might be given to microglial actions that facilitate neuronal repair after inflammatory damage.

As with the analysis of brain regional differences, the present results on the effects of disease state also highlight the utility of cell-specific, rather than brain homogenate approaches to expression studies. For example, recent AD research based on human brain homogenates has suggested critical hypermethylation changes of the *ANK1* gene (De Jager et al., 2014; Lunnon et al., 2014), one of the few transcripts in our study that was commonly altered in both AD and PD. As noted by the authors (De Jager et al., 2014; Lunnon et al., 2014), lacking cell specificity they could only speculate that their *ANK1* findings were related to activation of microglia through association with *PTK2B*, a gene associated with many microglial processes (Eleniste et al., 2016; Giralt et al., 2016; Jin et al., 2016; Meng et al., 2016; Morbach et al., 2016; Vanarotti et al., 2016; Zhang et al., 2016; Zhao et al., 2016). Our cell-specific results may help clarify and extend these findings by demonstrating that, indeed, *ANK1* is significantly up-regulated in AD compared to NC microglia, and that such upregulation may be a common feature in both AD and PD (Mastroeni et al., 2017).

Analyses of our RNAseq data also indicate significant changes in expression of a number of transcripts under the umbrella of viral processing (GO.0016032) (Table 2). Persistent viral infection in the AD brain has been reported (Bancher et al., 1996; Hill et al., 2014; Itzhaki, 2004; Itzhaki, 2014; Itzhaki et al., 2016; Jamieson et al., 1991; Lin et al., 1996; Martin et al., 2011; Walker et al., 1989), including a potential role for microglia in viral clearance (Koutsouras et al., 2016; Rock et al., 2004). More generally, there have been multiple reports suggesting viral (or bacterial or fungal) involvement in the etiology of AD (summarized in (Itzhaki et al., 2016). Although most studies to date have focused on herpes viruses, chlamydia, and select bacteria (reviewed in (Itzhaki et al., 2016), HBV infection is also detectable in brain, specifically in cirrhosis or hepatocarcinoma patients (Beretta et al., 2001; Choi et al., 2009; Kamimura et al., 2017; Pontisso et al., 1986; Post and Nagendra, 2009). Likewise, we now show that pathologically confirmed AD cases with persistent HBV infection exhibit clear HBV immunoreactivity in the pathologically-vulnerable CA1. Though speculative, the increasing HBV immunoreactivity in NC versus MCI versus AD cases in our study may suggest that if HBV infection reaches the brain, it could become a significant player in AD pathogenesis. Further studies with many more cases would be needed to support this hypothesis.

Whether or not the present findings reflect microglial responses to viruses such as HBV or represent a set of unrelated responses that happen to be common to viral processes also remains to be determined. It would be of interest, for example, to investigate whether or not prospective infection with HBV in an appropriate animal host would produce the same pattern of microglial gene expression changes as were observed here. Moreover, the same molecular machinery engaged during a viral infection could well be engaged in neurodegeneration. This

373 may be particularly pertinent with regard to microglia, considering their role in both viral
374 clearance and clearance of disease associated pathologies.
375
376
377 **Acknowledgments:** The authors declare no competing financial or conflict of interests. We are
378 grateful to the Banner Sun Health Research Institute Brain and Body Donation Program of Sun
379 City, Arizona for the provision of human brain samples. This work was supported by NIRG-15-
380 321390 and ADHS16-104646 FY2015-16 to D.M.
381
382
383 **References:**
384

385 Alam, Q., Alam, M.Z., Mushtaq, G., Damanhouri, G.A., Rasool, M., Kamal, M.A., Haque, A.,
386 2016. Inflammatory Process in Alzheimer's and Parkinson's Diseases: Central Role of Cytokines.
387 Curr Pharm Des 22(5), 541-548.
388 Alarcon, V., Hernandez, S., Rubio, L., Alvarez, F., Flores, Y., Varas-Godoy, M., De Ferrari,
389 G.V., Kann, M., Villanueva, R.A., Loyola, A., 2016. The enzymes LSD1 and Set1A cooperate
390 with the viral protein HBx to establish an active hepatitis B viral chromatin state. Sci Rep 6,
391 25901.
392 Bancher, C., Leitner, H., Jellinger, K., Eder, H., Setinek, U., Fischer, P., Wegiel, J., Wisniewski,
393 H.M., 1996. On the relationship between measles virus and Alzheimer neurofibrillary tangles in
394 subacute sclerosing panencephalitis. Neurobiol Aging 17(4), 527-533.
395 Berchtold, N.C., Coleman, P.D., Cribbs, D.H., Rogers, J., Gillen, D.L., Cotman, C.W., 2013.
396 Synaptic genes are extensively downregulated across multiple brain regions in normal human
397 aging and Alzheimer's disease. Neurobiol Aging 34(6), 1653-1661.
398 Berchtold, N.C., Cribbs, D.H., Coleman, P.D., Rogers, J., Head, E., Kim, R., Beach, T., Miller,
399 C., Troncoso, J., Trojanowski, J.Q., Zielke, H.R., Cotman, C.W., 2008. Gene expression changes
400 in the course of normal brain aging are sexually dimorphic. Proc Natl Acad Sci U S A 105(40),
401 15605-15610.
402 Berchtold, N.C., Sabbagh, M.N., Beach, T.G., Kim, R.C., Cribbs, D.H., Cotman, C.W., 2014.
403 Brain gene expression patterns differentiate mild cognitive impairment from normal aged and
404 Alzheimer's disease. Neurobiol Aging 35(9), 1961-1972.
405 Beretta, L., Caronni, M., Vanoli, M., Scorza, R., 2001. Churg-Strauss vasculitis with brain
406 involvement following hepatitis B vaccination. Clin Exp Rheumatol 19(6), 757.

Boche, D., Perry, V.H., Nicoll, J.A., 2013. Review: activation patterns of microglia and their identification in the human brain. Neuropathol Appl Neurobiol 39(1), 3-18.

Cahoy, J.D., Emery, B., Kaushal, A., Foo, L.C., Zamanian, J.L., Christopherson, K.S., Xing, Y., Lubischer, J.L., Krieg, P.A., Krupenko, S.A., Thompson, W.J., Barres, B.A., 2008. A transcriptome database for astrocytes, neurons, and oligodendrocytes: a new resource for understanding brain development and function. J Neurosci 28(1), 264-278.

Carpenter, A.F., Carpenter, P.W., Markesbery, W.R., 1993. Morphometric analysis of microglia in Alzheimer's disease. J Neuropathol Exp Neurol 52(6), 601-608.

Choi, H.J., Cho, B.C., Sohn, J.H., Shin, S.J., Kim, S.H., Kim, J.H., Yoo, N.C., 2009. Brain metastases from hepatocellular carcinoma: prognostic factors and outcome: brain metastasis from HCC. J Neurooncol 91(3), 307-313.

De Jager, P.L., Srivastava, G., Lunnon, K., Burgess, J., Schalkwyk, L.C., Yu, L., Eaton, M.L., Keenan, B.T., Ernst, J., McCabe, C., Tang, A., Raj, T., Replogle, J., Brodeur, W., Gabriel, S., Chai, H.S., Younkin, C., Younkin, S.G., Zou, F., Szyf, M., Epstein, C.B., Schneider, J.A., Bernstein, B.E., Meissner, A., Ertekin-Taner, N., Chibnik, L.B., Kellis, M., Mill, J., Bennett, D.A., 2014. Alzheimer's disease: early alterations in brain DNA methylation at ANK1, BIN1, RHBDF2 and other loci. Nat Neurosci 17(9), 1156-1163.

De Lucia, C., Rinchon, A., Olmos-Alonso, A., Riecken, K., Fehse, B., Boche, D., Perry, V.H., Gomez-Nicola, D., 2016. Microglia regulate hippocampal neurogenesis during chronic neurodegeneration. Brain Behav Immun 55, 179-190.

Di Scala, M., Otano, I., Gil-Farina, I., Vanrell, L., Hommel, M., Olague, C., Vales, A., Galarraga, M., Guembe, L., Ortiz de Solorzano, C., Ghosh, I., Maini, M.K., Prieto, J., Gonzalez-Aseguinolaza, G., 2016. Complementary Effects of Interleukin-15 and Alpha Interferon Induce Immunity in Hepatitis B Virus Transgenic Mice. J Virol 90(19), 8563-8574.

Durrenberger, P.F., Fernando, S., Kashefi, S.N., Ferrer, I., Hauw, J.J., Seilhean, D., Smith, C., Walker, R., Al-Sarraj, S., Troakes, C., Palkovits, M., Kasztner, M., Huitinga, I., Arzberger, T., Dexter, D.T., Kretzschmar, H., Reynolds, R., 2010. Effects of antemortem and postmortem variables on human brain mRNA quality: a BrainNet Europe study. J Neuropathol Exp Neurol 69(1), 70-81.

Eleniste, P.P., Patel, V., Posritong, S., Zero, O., Largura, H., Cheng, Y.H., Himes, E.R., Hamilton, M., Baughman, J., Kacena, M.A., Bruzzaniti, A., 2016. Pyk2 and Megakaryocytes Regulate Osteoblast Differentiation and Migration Via Distinct and Overlapping Mechanisms. J Cell Biochem 117(6), 1396-1406.

Farina, C., Aloisi, F., Meinl, E., 2007. Astrocytes are active players in cerebral innate immunity. Trends in immunology 28(3), 138-145.

Frost, J.L., Schafer, D.P., 2016. Microglia: Architects of the Developing Nervous System. Trends Cell Biol 26(8), 587-597.

Giralt, A., Coura, R., Girault, J.A., 2016. Pyk2 is essential for astrocytes mobility following brain lesion. Glia 64(4), 620-634.

Hill, J.M., Clement, C., Pogue, A.I., Bhattacharjee, S., Zhao, Y., Lukiw, W.J., 2014. Pathogenic microbes, the microbiome, and Alzheimer's disease (AD). Front Aging Neurosci 6, 127.

Hong, S., Beja-Glasser, V.F., Nfonoyim, B.M., Frouin, A., Li, S., Ramakrishnan, S., Merry, K.M., Shi, Q., Rosenthal, A., Barres, B.A., Lemere, C.A., Selkoe, D.J., Stevens, B., 2016. Complement and microglia mediate early synapse loss in Alzheimer mouse models. Science 352(6286), 712-716.

Itzhaki, R., 2004. Herpes simplex virus type 1, apolipoprotein E and Alzheimer' disease. Herpes 11 Suppl 2, 77A-82A.
Itzhaki, R.F., 2014. Herpes simplex virus type 1 and Alzheimer's disease: increasing evidence for a major role of the virus. Front Aging Neurosci 6, 202.
Itzhaki, R.F., Lathe, R., Balin, B.J., Ball, M.J., Bearer, E.L., Braak, H., Bullido, M.J., Carter, C., Clerici, M., Cosby, S.L., Del Tredici, K., Field, H., Fulop, T., Grassi, C., Griffin, W.S., Haas, J., Hudson, A.P., Kamer, A.R., Kell, D.B., Licastro, F., Letenneur, L., Lovheim, H., Mancuso, R., Miklossy, J., Otth, C., Palamara, A.T., Perry, G., Preston, C., Pretorius, E., Strandberg, T., Tabet, N., Taylor-Robinson, S.D., Whittum-Hudson, J.A., 2016. Microbes and Alzheimer's Disease. J Alzheimers Dis 51(4), 979-984.
Jamieson, G.A., Maitland, N.J., Wilcock, G.K., Craske, J., Itzhaki, R.F., 1991. Latent herpes simplex virus type 1 in normal and Alzheimer's disease brains. J Med Virol 33(4), 224-227.
Jin, W.J., Kim, B., Kim, J.W., Kim, H.H., Ha, H., Lee, Z.H., 2016. Notch2 signaling promotes osteoclast resorption via activation of PYK2. Cell Signal 28(5), 357-365.
Kamimura, K., Kobayashi, Y., Takahashi, Y., Abe, H., Kumaki, D., Yokoo, T., Kamimura, H., Sakai, N., Sakamaki, A., Abe, S., Takamura, M., Kawai, H., Yamagiwa, S., Terai, S., 2017. Tumor Markers for Early Diagnosis for Brain Metastasis of Hepatocellular Carcinoma: a Case Series and Literature Review for Effective Loco-regional Treatment. Cancer Biol Ther, 0.
Kettenmann, H., Hanisch, U.K., Noda, M., Verkhratsky, A., 2011. Physiology of microglia. Physiol Rev 91(2), 461-553.
Kettenmann, H., Kirchhoff, F., Verkhratsky, A., 2013. Microglia: new roles for the synaptic stripper. Neuron 77(1), 10-18.
Koutsouras, G.W., Ramos, R.L., Martinez, L.R., 2016. Role of microglia in fungal infections of the central nervous system. Virulence, 1-14.
Liang, W.S., Dunckley, T., Beach, T.G., Grover, A., Mastroeni, D., Ramsey, K., Caselli, R.J., Kukull, W.A., McKeel, D., Morris, J.C., Hulette, C.M., Schmechel, D., Reiman, E.M., Rogers, J., Stephan, D.A., 2008. Altered neuronal gene expression in brain regions differentially affected by Alzheimer's disease: a reference data set. Physiol Genomics 33(2), 240-256.
Lin, W.R., Shang, D., Itzhaki, R.F., 1996. Neurotropic viruses and Alzheimer disease. Interaction of herpes simplex type 1 virus and apolipoprotein E in the etiology of the disease. Mol Chem Neuropathol 28(1-3), 135-141.
Liu, Y., Walter, S., Stagi, M., Cherny, D., Letiembre, M., Schulz-Schaeffer, W., Heine, H., Penke, B., Neumann, H., Fassbender, K., 2005. LPS receptor (CD14): a receptor for phagocytosis of Alzheimer's amyloid peptide. Brain 128(Pt 8), 1778-1789.
Lopes, C.T., Franz, M., Kazi, F., Donaldson, S.L., Morris, Q., Bader, G.D., 2010. Cytoscape Web: an interactive web-based network browser. Bioinformatics 26(18), 2347-2348.
Lunnon, K., Smith, R., Hannon, E., De Jager, P.L., Srivastava, G., Volta, M., Troakes, C., Al-Sarraj, S., Burrage, J., Macdonald, R., Condliffe, D., Harries, L.W., Katsel, P., Haroutunian, V., Kaminsky, Z., Joachim, C., Powell, J., Lovestone, S., Bennett, D.A., Schalkwyk, L.C., Mill, J., 2014. Methylomic profiling implicates cortical deregulation of ANK1 in Alzheimer's disease. Nat Neurosci 17(9), 1164-1170.
Luo, C., Ikegaya, Y., Koyama, R., 2016. Microglia and neurogenesis in the epileptic dentate gyrus. Neurogenesis (Austin) 3(1), e1235525.
Mandybur, T.I., Chuirazzi, C.C., 1990. Astrocytes and the plaques of Alzheimer's disease. Neurology 40(4), 635-639.

Martin, C., Solis, L., Concha, M.I., Otth, C., 2011. [Herpes simplex virus type 1 as risk factor associated to Alzheimer disease]. Rev Med Chil 139(6), 779-786.

Mastroeni, D., Khdour, O.M., Delvaux, E., Nolz, J., Olsen, G., Berchtold, N., Cotman, C., Hecht, S.M., Coleman, P.D., 2016. Nuclear but not mitochondrial-encoded OXPHOS genes are altered in aging, mild cognitive impairment, and Alzheimer's disease. Alzheimers Dement.

Mastroeni, D., Sekar, S., Nolz, J., Delvaux, E., Lunnon, K., Mill, J., Liang, W.S., Coleman, P.D., 2017. ANK1 is up-regulated in laser captured microglia in Alzheimer's brain; the importance of addressing cellular heterogeneity. PLoS One 12(7), e0177814.

Meng, X.Q., Dai, Y.Y., Jing, L.D., Bai, J., Liu, S.Z., Zheng, K.G., Pan, J., 2016. Subcellular localization of Pyk2 during oocyte fertilization and early-embryo development in mice. J Reprod Dev.

Morbach, H., Schickel, J.N., Cunningham-Rundles, C., Conley, M.E., Reisli, I., Franco, J.L., Meffre, E., 2016. CD19 controls Toll-like receptor 9 responses in human B cells. J Allergy Clin Immunol 137(3), 889-898 e886.

Murray, K., Bruce, S.A., Hinnen, A., Wingfield, P., van Erd, P.M., de Reus, A., Schellekens, H., 1984. Hepatitis B virus antigens made in microbial cells immunise against viral infection. EMBO J 3(3), 645-650.

Padurariu, M., Ciobica, A., Mavroudis, I., Fotiou, D., Baloyannis, S., 2012. Hippocampal neuronal loss in the CA1 and CA3 areas of Alzheimer's disease patients. Psychiatr Danub 24(2), 152-158.

Paolicelli, R.C., Bolasco, G., Pagani, F., Maggi, L., Scianni, M., Panzanelli, P., Giustetto, M., Ferreira, T.A., Guiducci, E., Dumas, L., Ragozzino, D., Gross, C.T., 2011. Synaptic pruning by microglia is necessary for normal brain development. Science 333(6048), 1456-1458.

Parachikova, A., Agadjanyan, M.G., Cribbs, D.H., Blurton-Jones, M., Perreau, V., Rogers, J., Beach, T.G., Cotman, C.W., 2007. Inflammatory changes parallel the early stages of Alzheimer disease. Neurobiol Aging 28(12), 1821-1833.

Perry, V.H., O'Connor, V., 2010. The role of microglia in synaptic stripping and synaptic degeneration: a revised perspective. ASN Neuro 2(5), e00047.

Pikhovych, A., Stolberg, N.P., Jessica Flitsch, L., Walter, H.L., Graf, R., Fink, G.R., Schroeter, M., Rueger, M.A., 2016. Transcranial Direct Current Stimulation Modulates Neurogenesis and Microglia Activation in the Mouse Brain. Stem Cells Int 2016, 2715196.

Pontisso, P., Schiavon, E., Alberti, A., Realdi, G., Locasciulli, A., Masera, G., 1986. Does hepatitis B virus cross the blood-brain barrier? N Engl J Med 314(8), 518-519.

Post, A., Nagendra, S., 2009. Reactivation of hepatitis B: pathogenesis and clinical implications. Curr Infect Dis Rep 11(2), 113-119.

Rivest, S., 2009. Regulation of innate immune responses in the brain. Nature reviews. Immunology 9(6), 429-439.

Rock, R.B., Gekker, G., Hu, S., Sheng, W.S., Cheeran, M., Lokensgard, J.R., Peterson, P.K., 2004. Role of microglia in central nervous system infections. Clin Microbiol Rev 17(4), 942-964, table of contents.

Rogers, J., Mastroeni, D., Leonard, B., Joyce, J., Grover, A., 2007. Neuroinflammation in Alzheimer's disease and Parkinson's disease: are microglia pathogenic in either disorder? Int Rev Neurobiol 82, 235-246.

Rogers, J., Webster, S., Lue, L.F., Brachova, L., Civin, W.H., Emmerling, M., Shivers, B., Walker, D., McGeer, P., 1996. Inflammation and Alzheimer's disease pathogenesis. Neurobiol Aging 17(5), 681-686.

Schafer, D.P., Stevens, B., 2015. Microglia Function in Central Nervous System Development and Plasticity. Cold Spring Harb Perspect Biol 7(10), a020545.
Shigemoto-Mogami, Y., Hoshikawa, K., Goldman, J.E., Sekino, Y., Sato, K., 2014. Microglia enhance neurogenesis and oligodendrogenesis in the early postnatal subventricular zone. J Neurosci 34(6), 2231-2243.
Sierra, A., Encinas, J.M., Deudero, J.J., Chancey, J.H., Enikolopov, G., Overstreet-Wadiche, L.S., Tsirka, S.E., Maletic-Savatic, M., 2010. Microglia shape adult hippocampal neurogenesis through apoptosis-coupled phagocytosis. Cell Stem Cell 7(4), 483-495.
Solito, E., Sastre, M., 2012. Microglia function in Alzheimer's disease. Front Pharmacol 3, 14.
Stahl, S., MacKay, P., Magazin, M., Bruce, S.A., Murray, K., 1982. Hepatitis B virus core antigen: synthesis in Escherichia coli and application in diagnosis. Proc Natl Acad Sci U S A 79(5), 1606-1610.
Szklarczyk, D., Morris, J.H., Cook, H., Kuhn, M., Wyder, S., Simonovic, M., Santos, A., Doncheva, N.T., Roth, A., Bork, P., Jensen, L.J., von Mering, C., 2017. The STRING database in 2017: quality-controlled protein-protein association networks, made broadly accessible. Nucleic Acids Res 45(D1), D362-D368.
Tobinick, E., 2009. Tumour necrosis factor modulation for treatment of Alzheimer's disease: rationale and current evidence. CNS Drugs 23(9), 713-725.
Trapnell, C., Pachter, L., Salzberg, S.L., 2009. TopHat: discovering splice junctions with RNA-Seq. Bioinformatics 25(9), 1105-1111.
Trapnell, C., Roberts, A., Goff, L., Pertea, G., Kim, D., Kelley, D.R., Pimentel, H., Salzberg, S.L., Rinn, J.L., Pachter, L., 2012. Differential gene and transcript expression analysis of RNA-seq experiments with TopHat and Cufflinks. Nature protocols 7(3), 562-578.
Vanarotti, M.S., Finkelstein, D.B., Guibao, C.D., Nourse, A., Miller, D.J., Zheng, J.J., 2016. Structural Basis for the Interaction between Pyk2-FAT Domain and Leupaxin LD Repeats. Biochemistry 55(9), 1332-1345.
Walker, D.G., Lue, L.F., 2015. Immune phenotypes of microglia in human neurodegenerative disease: challenges to detecting microglial polarization in human brains. Alzheimers Res Ther 7(1), 56.
Walker, D.G., O'Kusky, J.R., McGeer, P.L., 1989. In situ hybridization analysis for herpes simplex virus nucleic acids in Alzheimer disease. Alzheimer Dis Assoc Disord 3(3), 123-131.
Wyss-Coray, T., Rogers, J., 2012. Inflammation in Alzheimer disease-a brief review of the basic science and clinical literature. Cold Spring Harb Perspect Med 2(1), a006346.
Zhang, Z., Chu, S.F., Mou, Z., Gao, Y., Wang, Z.Z., Wei, G.N., Chen, N.H., 2016. Ganglioside GQ1b induces dopamine release through the activation of Pyk2. Mol Cell Neurosci 71, 102-113.
Zhao, M., Finlay, D., Zharkikh, I., Vuori, K., 2016. Novel Role of Src in Priming Pyk2 Phosphorylation. PLoS One 11(2), e0149231.

Figure Legends:

Table 1: List of the significant *(p<.05)* 65 viral-associated genes and respective log2 fold changes identified in AD CA1 compared to NC subjects.

Figure 1: Microglia exhibit different expression profiles in different brain regions of the non-diseased human elderly brain. Heat maps of the significant *(p<.05)* log2 fold changes in non-demented elderly control microglia within two brain regions, CA1 of the hippocampus and substantia nigra (SN), demonstrate unique expression profiles within regions. Heuristic cluster analysis of cluster 1 vs. cluster 2, or NC CA1 vs NC SN reveal three significant (*p<.05, FDR<.02*), upregulated biological processes in NC CA1 microglia: nervous system development, regulation of neuronal synaptic plasticity, and neurogenesis. Further analysis in the same subjects, cluster 3 vs. cluster 4, shows highly significant (*p<.05, FDR<.000000000001)* log2 fold changes in genes associated with mitochondrial function.

Figure 2: Microglia exhibit different expression profiles in CA1 of the diseased human brain. Heat maps are provided that represent the significant *(p<.05*) log2 fold changes in laser capture microglia from AD and PD cases compared to NC patients. A,B) Heuristic heat map illustrations of differentially expressed (log2 fold changes) in genes in AD CA1 vs. NC CA1 (A) and PD CA1 vs. NC CA1 (B). C) Pathway Analysis (2D-single cluster analysis) using Cytoscape network visualizer. The pie charts depict molecular interaction network and biological pathways in AD CA1 (C) and PD CA1 (D). C) 367 significant (p<.01-Bonferroni step down correction) genes were used in the pathway analysis for AD/NC comparisons. The top three pathways in AD microglia were thyroid hormone synthesis, icosanoid metabolic process, and regulation of viral process. D) 409 significant (p<.01-Bonferroni step down correction) genes were used in the pathway analysis for PD/NC comparisons. The top three pathways in PD microglia were aldosterone synthesis and secretion, positive regulation of protein complex assembly, and focal adhesion assembly.

608 **Figure 3**: Microglia exhibit different expression profiles in different regions of the diseased
609 human brain. Heat maps are shown that illustrate the significant *(p<.05*) log2 fold changes in a
610 heuristic hierarchical clustering output from laser capture microglia from AD and PD brain. A) A
611 heat map, within group comparison (e.g. AD CA1 vs. AD SN) reveals 100 differentially
612 expressed genes in laser captured microglial cells. Analysis of the log2 fold changes between
613 cluster 1 and cluster 2 identifies three significant (*p<.05*, *FDR<.002*) processes: synaptic
614 transmission, cell-cell signaling, and metal ion transport. Comparison of cluster 3 and cluster 4
615 shows no significant biological pathway. B) 313 significantly altered, log2 fold changes were
616 found in PD CA1 vs. PD SN. Cluster analysis—cluster 1 versus cluster 3—shows three
617 significant (*p<.05*, FDR<.00000001) biological processes: behavior, regulation of transport, and,
618 like AD, synaptic transmission. No significant biological pathways were identified for cluster 3
619 and cluster 4.
620 **Figure 4:** Percent of viral associated genes in laser capture microglia. AD and PD microglia
621 were both compared to age-matched NC subjects. Signficant alterations in viral-associated
622 transcripts were some 5-fold more common in AD CA1 than in PD CA1, AD SN, or PD SN.
623 **Figure 5:** Representative photomicrographs of HBV core immunoreactivity in hippocampus
624 CA1 in a Braak I NC subject (A), Braak IV MCI subject (B), and Braak V AD subject (C).
625 **Supplementary Table 1:** Detailed demographic data from NC, AD and PD subjects included in
626 the laser capture and immunohistochemistry studies.
627 **Supplementary Table 2:** Top 100 genes significantly *(p<0.05)* altered in AD CA1 microglia
628 and PD CA1 microglia compared to microglia in age-matched control subjects.
629 **Supplementary Table 3:** A) Functional enrichment analysis and B) KEGG pathways identified
630 in CA1 microglia compared to normal control subjects.

Supplementary Figure 1: Schematic and workflow of unbiased HBV identification.

Supplementary Figure 2: Schematic of laser capture microdissection of hippocampal tissue sections. (A) Hippocampal sections were immunoreacted using an antibody to HLA-DR. (B) ~600 HLA-DR positive microglia cells were captured. Individual microglial cells were cut and dropped into an inverted microcentrifuge cap (C) .

Supplementary Figure 3: Triplicate QPCR expression data for relative expression levels of the microglial-specific transcripts CD14, CD68, and CD11b (Liu et al., 2005; Walker and Lue, 2015), the astrocyte-specific transcript GFAP (Mandybur and Chuirazzi, 1990), and the neuron-specific transcipts CHRM1, SYP, and MAP2 (Cahoy et al., 2008; Liang et al., 2008). These expression data show nearly complete microglial isolation within the samples, with little to no contamination from other cell types, as well as the ability to amplify transcripts from a small number of identified cells without confounding by other cell types.

Supplementary Figure 4: Quality control measures. A) Total number of reads per sample and B) percent mapped reads and percent duplication.

Supplementary Figure 5: Quality control measures: A) Percent mRNA and intergenic, intronic and ribosomal bases identified in RNA sequencing data. B) Representation of the median 5' and 3' biases.

Supplementary Figure 6: Quality control measures: A) Library insert size distributions: Representative graphs of the distribution of insert sizes for each library. We expect approximately 150-250bp long inserts. B) Quality score distribution: Representative graphs of the distribution of quality scores for each library. Quality scores are on a pared scale such that a score of 30 indicates 99.9% base call accuracy

Supplementary Figure 7: Known and Predicted Protein-Protein Interactions within the top 100 genes using string software. Visual protein interaction of the top 100 significant genes with a *p-value <0.01* in AD CA1 vs. NC CA1 (A) and (B) PD CA1 vs. NC CA1. Detailed information regarding the top 100 genes can been found in Supplementary Table 2.

Supplementary Figure 8: Overlapping Genes in PD CA1, PD SN, and AD SN compared to AD CA1. Fifteen of the 65 differentially expressed genes within GO.0016032 (viral process) identified in AD CA1 microglia were also significantly changed in PD CA1 microglia, as were five in AD SN and two in PD SN.

Supplementary Figure 9: String protein interactions of the 65 viral-associated genes in AD CA1 microglia (Table 1) depicted by colored nodes (first shell interactions). Known interactions derived from both curated databases and experimentally determined interactions predicted the strongest association with viral processes GO.0016032 (FDR =6.90E^{-38}).

Table 1: List of the significant *(p<.05)* 65 viral-associated genes and respective log2 fold changes identified in AD CA1 compared to NC subjects.

Gene ID	Gene Name	Gene Discription	Fold Change
ENSG00000197122	SRC	v-src avian sarcoma (Schmidt-Ruppin A-2) viral oncogene homolog [Source:HGNC Symbol;Acc:11283]	-4.552012242
ENSG00000134058	CDK7	cyclin-dependent kinase 7 [Source:HGNC Symbol;Acc:1778]	-4.076830618
ENSG00000167701	GPT	glutamic-pyruvate transaminase (alanine aminotransferase) [Source:HGNC Symbol;Acc:4552]	-4.07370501
ENSG00000111331	OAS3	2'-5'-oligoadenylate synthetase 3, 100kDa [Source:HGNC Symbol;Acc:8088]	-3.993370726
ENSG00000187608	ISG15	ISG15 ubiquitin-like modifier [Source:HGNC Symbol;Acc:4053]	-3.987143039
ENSG00000130164	LDLR	low density lipoprotein receptor [Source:HGNC Symbol;Acc:6547]	-3.967429836
ENSG00000068001	HYAL2	hyaluronoglucosaminidase 2 [Source:HGNC Symbol;Acc:5321]	-3.904386945
ENSG00000100902	PSMA6	proteasome (prosome, macropain) subunit, alpha type, 6 [Source:HGNC Symbol;Acc:9535]	-3.656944614
ENSG00000181026	AEN*	apoptosis enhancing nuclease [Source:HGNC Symbol;Acc:25722]	-3.420039156
ENSG00000137274	BPHL	biphenyl hydrolase-like (serine hydrolase) [Source:HGNC Symbol;Acc:1094]	-3.384573936
ENSG00000160791	CCR5*	chemokine (C-C motif) receptor 5 (gene/pseudogene) [Source:HGNC	-3.319029326

		Symbol;Acc:1606]	
ENSG00000143319	ISG20L2	interferon stimulated exonuclease gene 20kDa-like 2 [Source:HGNC Symbol;Acc:25745]	-3.304407584
ENSG00000115267	IFIH1	interferon induced with helicase C domain 1 [Source:HGNC Symbol;Acc:18873]	-3.255977918
ENSG00000184990	SIVA1	SIVA1, apoptosis-inducing factor [Source:HGNC Symbol;Acc:17712]	-3.168329509
ENSG00000136986	DERL1	derlin 1 [Source:HGNC Symbol;Acc:28454]	-3.008998244
ENSG00000102886	GDPD3	glycerophosphodiester phosphodiesterase domain containing 3 [Source:HGNC Symbol;Acc:28638]	-2.865699484
ENSG00000060069	CTDP1	CTD (carboxy-terminal domain, RNA polymerase II, polypeptide A) phosphatase, subunit 1 [Source:HGNC Symbol;Acc:2498]	-2.807618162
ENSG00000161057	PSMC2	proteasome (prosome, macropain) 26S subunit, ATPase, 2 [Source:HGNC Symbol;Acc:9548]	-2.709368462
ENSG00000166266	CUL5	cullin 5 [Source:HGNC Symbol;Acc:2556]	-2.704201444
ENSG00000138346	DNA2	DNA replication helicase/nuclease 2 [Source:HGNC Symbol;Acc:2939]	-2.621416609
ENSG00000186468	RPS23	ribosomal protein S23 [Source:HGNC Symbol;Acc:10410]	-2.529189573
ENSG00000169871	TRIM56	tripartite motif containing 56 [Source:HGNC Symbol;Acc:19028]	-2.435195358
ENSG00000126456	IRF3	interferon regulatory factor 3 [Source:HGNC Symbol;Acc:6118]	-2.279811099
ENSG00000185624	P4HB	prolyl 4-hydroxylase, beta polypeptide [Source:HGNC Symbol;Acc:8548]	-2.036493552
ENSG00000170889	RPS9	ribosomal protein S9 [Source:HGNC Symbol;Acc:10442]	-2.035795799
ENSG00000137076	TLN1	talin 1 [Source:HGNC Symbol;Acc:11845]	-1.933824787
ENSG00000175166	PSMD2	proteasome (prosome, macropain) 26S subunit, non-ATPase, 2 [Source:HGNC Symbol;Acc:9559]	-1.927802701
ENSG00000170653	ATF7	activating transcription factor 7 [Source:HGNC Symbol;Acc:792]	-1.899645579
ENSG00000204713	TRIM27	tripartite motif containing 27 [Source:HGNC Symbol;Acc:9975]	-1.896345577
ENSG00000142453	CARM1	coactivator-associated arginine methyltransferase 1 [Source:HGNC Symbol;Acc:23393]	-1.834673238
ENSG00000204389	HSPA1A	heat shock 70kDa protein 1A [Source:HGNC Symbol;Acc:5232]	-1.828274094
ENSG00000092847	AGO1	argonaute RISC catalytic component 1 [Source:HGNC Symbol;Acc:3262]	-1.594708889
ENSG00000033800	PIAS1	protein inhibitor of activated STAT, 1 [Source:HGNC Symbol;Acc:2752]	-1.521557046
ENSG00000114166	KAT2B	K(lysine) acetyltransferase 2B [Source:HGNC Symbol;Acc:8638]	-1.432667577
ENSG00000136436	CALCOCO2	calcium binding and coiled-coil domain 2 [Source:HGNC Symbol;Acc:29912]	-1.430771501
ENSG00000120948	TARDBP	TAR DNA binding protein [Source:HGNC Symbol;Acc:11571]	-1.42080567
ENSG00000122406	RPL5	ribosomal protein L5 [Source:HGNC Symbol;Acc:10360]	-1.412980701
ENSG00000067560	RHOA	ras homolog family member A [Source:HGNC Symbol;Acc:667]	-1.210163167
ENSG00000132274	TRIM22	tripartite motif containing 22 [Source:HGNC Symbol;Acc:16379]	1.210244575
ENSG00000124164	VAPB	VAMP (vesicle-associated membrane protein)-associated protein B and C [Source:HGNC Symbol;Acc:12649]	1.259873133
ENSG00000110395	CBL	Cbl proto-oncogene, E3 ubiquitin protein ligase [Source:HGNC Symbol;Acc:1541]	1.534895565
ENSG00000095015	MAP3K1	mitogen-activated protein kinase kinase kinase 1, E3 ubiquitin protein ligase [Source:HGNC Symbol;Acc:6848]	1.535983096
ENSG00000113595	TRIM23	tripartite motif containing 23 [Source:HGNC Symbol;Acc:660]	1.72574717
ENSG00000063322	MED29	mediator complex subunit 29 [Source:HGNC Symbol;Acc:23074]	1.936409629
ENSG00000076248	UNG	uracil-DNA glycosylase [Source:HGNC Symbol;Acc:12572]	1.952332227
ENSG00000119912	IDE	insulin-degrading enzyme [Source:HGNC Symbol;Acc:5381]	2.038043499
ENSG00000116062	MSH6	mutS homolog 6 [Source:HGNC Symbol;Acc:7329]	2.046303008
ENSG00000149136	SSRP1	structure specific recognition protein 1 [Source:HGNC Symbol;Acc:11327]	2.142662805
ENSG00000189091	SF3B3	splicing factor 3b, subunit 3, 130kDa [Source:HGNC Symbol;Acc:10770]	2.25427061
ENSG00000138750	NUP54	nucleoporin 54kDa [Source:HGNC Symbol;Acc:17359]	2.28622086
ENSG00000139613	SMARCC2	SWI/SNF related, matrix associated, actin dependent regulator of chromatin, subfamily c, member 2 [Source:HGNC Symbol;Acc:11105]	2.328440377

ENSG00000101868	POLA1	polymerase (DNA directed), alpha 1, catalytic subunit [Source:HGNC Symbol;Acc:9173]	2.74799104
ENSG00000147457	CHMP7	charged multivesicular body protein 7 [Source:HGNC Symbol;Acc:28439]	2.771205206
ENSG00000128536	CDHR3	cadherin-related family member 3 [Source:HGNC Symbol;Acc:26308]	2.805397322
ENSG00000100353	EIF3D	eukaryotic translation initiation factor 3, subunit D [Source:HGNC Symbol;Acc:3278]	2.911057347
ENSG00000249853	HS3ST5	heparan sulfate (glucosamine) 3-O-sulfotransferase 5 [Source:HGNC Symbol;Acc:19419]	2.995508775
ENSG00000136997	MYC	v-myc avian myelocytomatosis viral oncogene homolog [Source:HGNC Symbol;Acc:7553]	3.055507235
ENSG00000171720	HDAC3	histone deacetylase 3 [Source:HGNC Symbol;Acc:4854]	3.234037794
ENSG00000146425	DYNLT 1	dynein, light chain, Tctex-type 1 [Source:HGNC Symbol;Acc:11697]	3.258469833
ENSG00000144231	POLR2 D	polymerase (RNA) II (DNA directed) polypeptide D [Source:HGNC Symbol;Acc:9191]	3.395242197
ENSG00000183853	PSMC3	kin of IRRE like (Drosophila) [Source:HGNC Symbol;Acc:15734]	3.449412673
ENSG00000101412	E2F1	E2F transcription factor 1 [Source:HGNC Symbol;Acc:3113]	3.612453322
ENSG00000163634	THOC7	THO complex 7 homolog (Drosophila) [Source:HGNC Symbol;Acc:29874]	3.852427434
ENSG00000180198	RCC1	regulator of chromosome condensation 1 [Source:HGNC Symbol;Acc:1913]	4.664535808

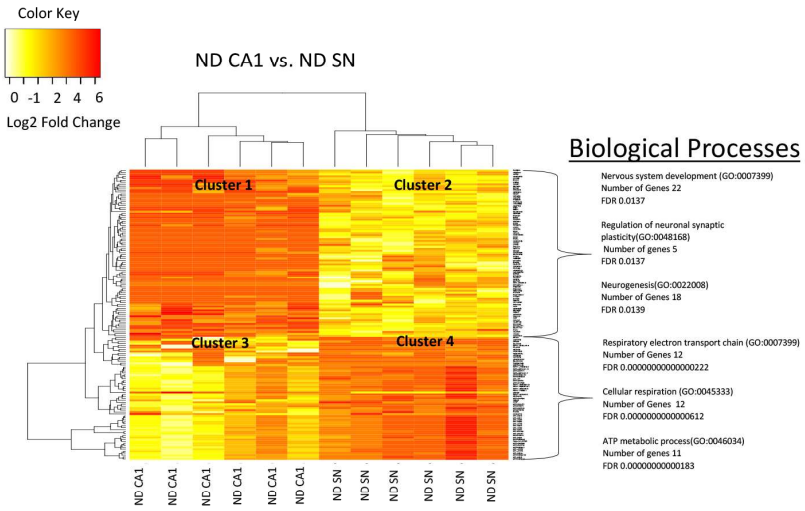

Mastroeni et al. Figure 2

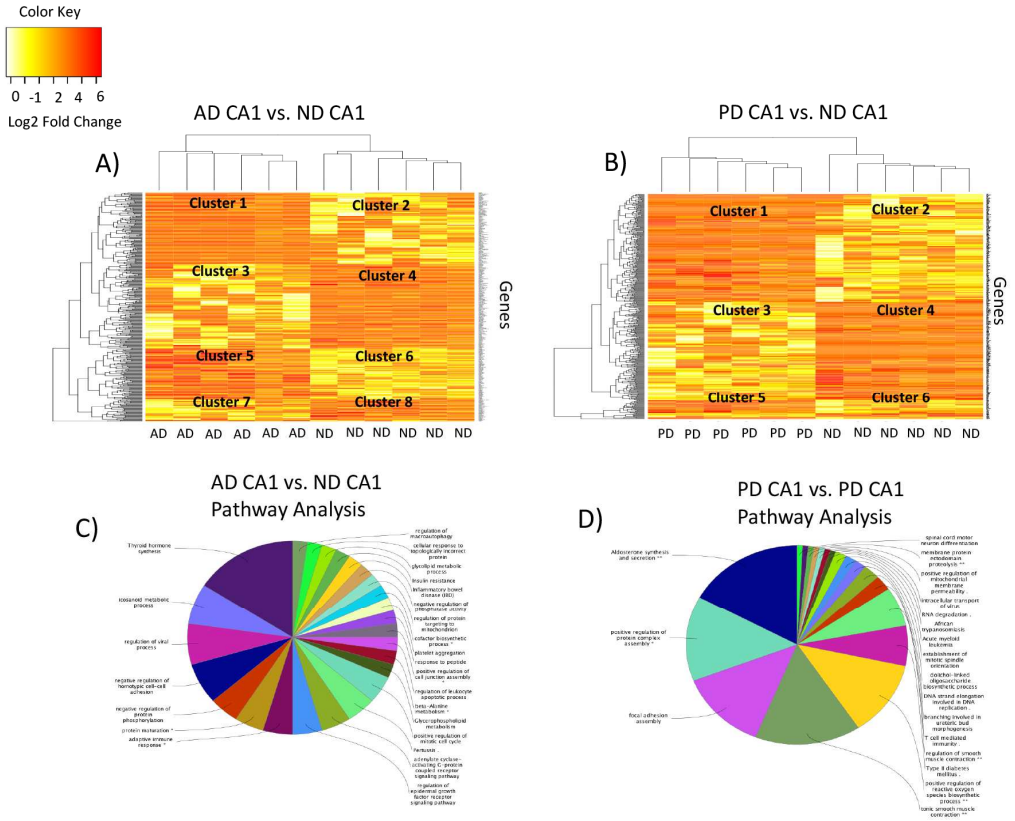

Mastroeni et al. Figure 3

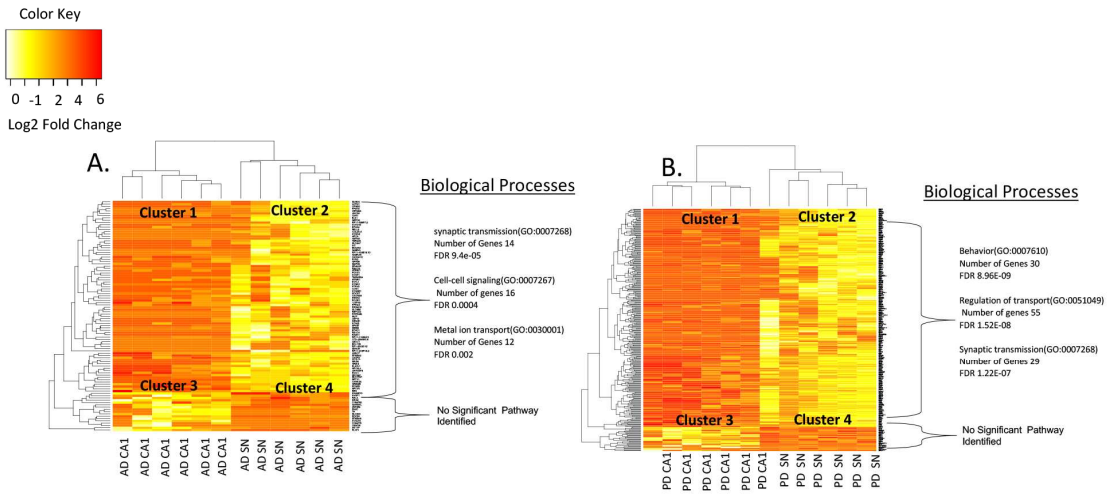

Mastroeni et al. Figure 4

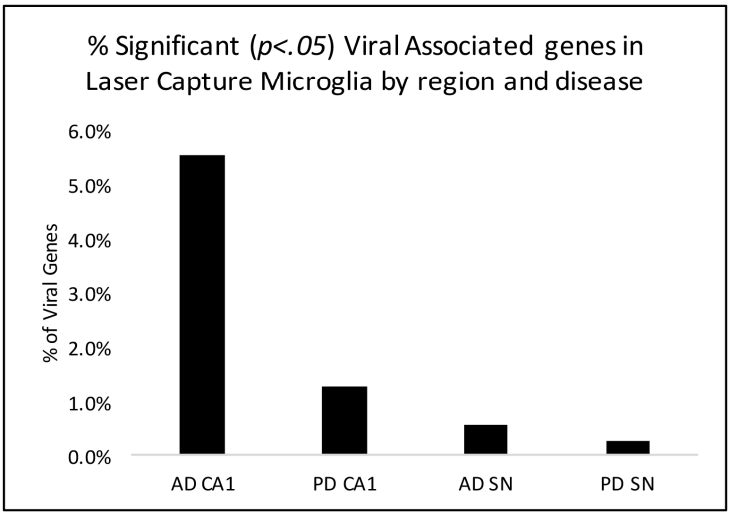

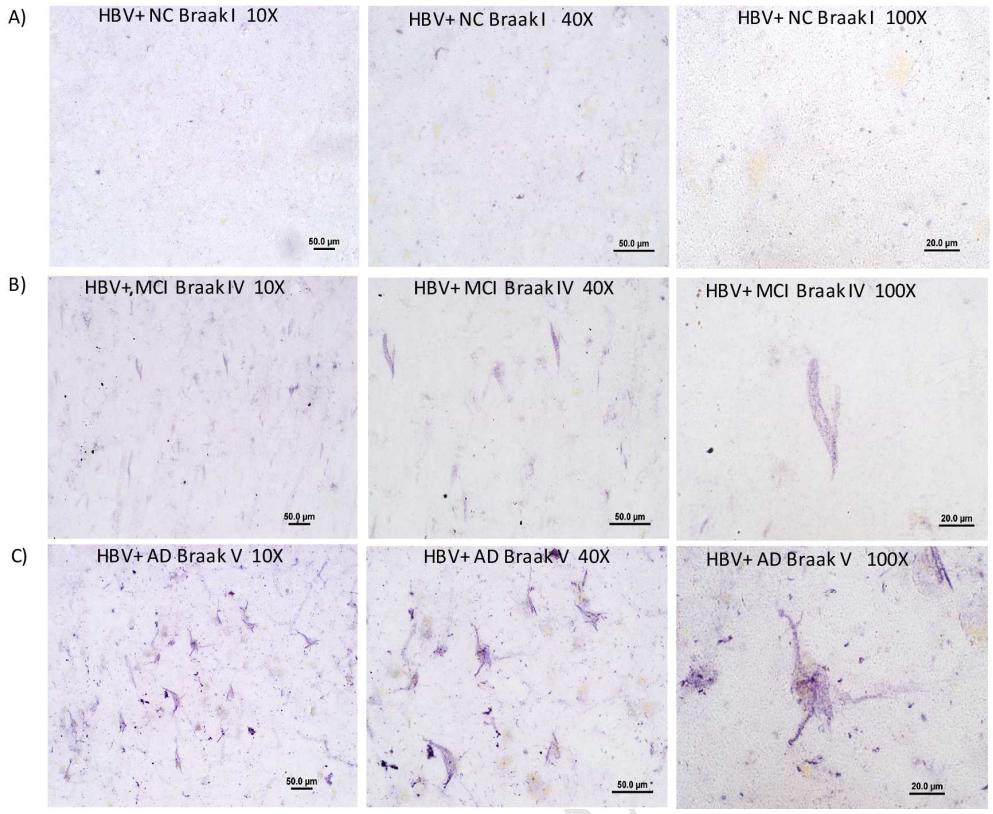

Highlights:

- Microglia expression profiles are unique depending on brain region in normal aging.
- Microglia exhibit unique expression profiles in different neurological diseases.
- Microglia in AD associated with a new role in neuronal repair and maintenance.
- Microglia expression profiles in AD identifies response to viruses.
- Increase risk for AD in hepatitis B carriers revealed in brain bank.

Verification:

All authors declare no conflict of interest.

None of the author's institution has contracts relating to this research through which it or any other organization may stand to gain financially now or in the future; including any other agreements of authors or their institutions that could be seen as involving a financial interest in this work.

All sources of financial support related to the manuscript have been included in the manuscript proper.

The data contained in the manuscript being submitted have not been previously published, have not been submitted elsewhere and will not be submitted elsewhere while under consideration at Neurobiology of Aging.

Appropriate approval and procedures concerning human subjects and animals are clearly stated in the manuscript proper.

All authors have reviewed the contents of the manuscript being submitted, approve of its contents and validate the accuracy of the data.